52nd CIRP Conference on Manufacturing Systems

Acoustic emission-based characterization of focal position during ultra-short pulse laser ablation

Andreas Kacaras[a],*, Matthias Bächle[b], Markus Schwabe[b], Frederik Zanger[a], Fernando Puente León[b], Volker Schulze[a]

[a]Institute of Production Science, Karlsruhe Institute of Technology, Kaiserstr. 12, 76131 Karlsruhe
[b]Institute of Industrial Information Technology, Karlsruhe Institute of Technology, Hertzstr. 16, 76187 Karlsruhe

* Corresponding author. Tel.: +49-721-608-44015 ; fax: +49-721-608-45004. E-mail address: Andreas.Kacaras@kit.edu

Abstract

Microstructures were ablated using an ultra-short pulse laser system in order to investigate the influence of focal position on the surface topography. In addition, acoustic emissions measured by a piezoelectric sensor adapted to the AISI 4140 workpiece were analyzed and correlated with the focal position and the resulting surface topography. Frequency ranges sensitive to variations of the z-axis position were determined by STFT analysis. Subsequently, significant signal components were processed to enable an inference about the focal position. The hypothesis of assessing the focal position in-process based on acoustic emissions to ensure high precision during laser ablation could be confirmed.

1. Introduction

Microfabrication by means of ultra-short pulse laser ablation is widely used in industry and science. Common applications are surface texturing in order to improve friction and wear [1,2] or the fabrication of micro mold inserts [3].

In order to achieve precisely ablated micro structures, melting effects for instance due to heat accumulation effects need to be avoided [4,5]. Moreover, the used energy density during laser ablation influences the ablation rate [4] and is highly dependent on deviations in the focal distance [6]. Therefore, a well-adjusted focal position is mandatory in order to achieve high quality ablated structures in terms of reproducibility and precision. The control of the focal position represents a major challenge especially for the machining of complex shaped workpieces [7]. Scientific articles focus on methods based on optical and acoustic emission signals.

Proposed techniques for the optical detection of the focal position are based on complex systems of optical elements consisting of beam splitters, lenses, apertures and detectors [6,8].

Fox et al. [8] proposed a technique which uses reflections caused by blackbody radiation in combination with chromatic aberration effects in order to measure the distance between workpiece and the focusing lens. This technique is not applicable to ultra-short pulse laser ablation since heating of workpiece material is unwanted.

Cao et al. presented an approach for real-time focal position detection using diffractive beam samplers (DBS) [9], investigations of the laser-beam profile [7] and double-hole masks [6], while using the same beam path for the fabrication laser and detection. However, the laser power had to be limited due to the same beam path [7,9]. Additionally, a calibration was, as in all optical systems, necessary [6,7].

The disadvantage of using optical methods during laser manufacturing is the creation of plasma, due to the high laser power, which can pollute the lens or create unwanted reflections [8,9]. Additionally, in ultra-short pulse laser ablation these need to be very sensitive and are therefore highly susceptible to errors in the beam path. Using acoustic emission signals these problems can be avoided.

Schulze et al. [10] proposed a method capable of automatic focal positioning for the ultra-short pulse laser ablation process by detection of air-borne acoustic emissions. Deviations of 50 μm between optically and acoustically detected focal positions have been demonstrated.

The analysis of solid-borne emissions has been addressed by Bordatchev and Nikumb [11]. The focal position has been classified by means of feature extraction and pattern recognition techniques demanding a large amount of training data from different machines in order to produce a reliable assessment of the focal position.

Solid-borne emissions provide a higher bandwidth and are less sensitive to environment noises. Therefore, this paper investigates the in-situ detection of focal position during laser ablation using solid-borne acoustic emission measurement with time-frequency analysis [12]. A novel method is introduced to improve the signal-to-noise ratio by exploiting the sequential laser ablation of material layers.

Nomenclature

a	ablated dimension projected in ablation direction
d_f	focal spot diameter
E	STFT of AE data
f	frequency
f_L	focal length of the f-theta lens
f_{rep}	pulse frequency
f_s	sample rate
h	structure depth
h_f	structure depth at focal position
I_{FR}	ablation intensity value
K	number of STFT frequency bins
k	discrete frequency index of STFT
m	discrete time index of STFT
N	number of discrete AE signal points
n	discrete time index of raw AE data
P	laser power
R	repetitions
S_{FR}	fourier transform of summed time signal s_{FR}
s_{FR}	summed time signal of defined frequency range
Sa	arithmetic average surface roughness
t	time
t_S	sample time
v	scan speed
w	structure width
w_f	structure width at focal position
x	raw AE data
z	z-axis position
z_f	focal position
γ	gaussian window function
λ	emitted wavelength of the laser beam

2. Experimental setup and procedure

AISI 4140 (EN steel 1.7225) in a quenched and tempered state (austenized at 850°C, quenched in oil and tempered at 450°C for 2 h) was used as workpiece material. After heat treatment surface grinding was performed resulting in an initial surface roughness of the workpiece of $Sa = 0.42 \pm 0.15$ μm. For laser ablation, the ultra-short pulse laser system TruMicro 5050 (Trumpf GmbH) with an average pulse duration of 6 ps was used. The focal diameter d_f of the laser beam being supposed as a Gaussian intensity distribution was estimated for a number of 100 pulses using the method proposed by Liu [13] and was calculated as $d_f = 38$ μm for $(1/e^2)$. For the estimation of d_f an accurately adjusted focal position z_f is mandatory. Therefore, the depths of dimples ablated with varied z-axis position were analyzed. The dimple showing the highest depth revealed z_f.

In order to experimentally determine the correlation between surface topography and z-axis position, microgrooves were ablated with varied z-axis positions and were analyzed in terms of structure depths h and widths w. Used process parameters during laser ablation are shown in Table 1.

Table 1. Process parameters during laser ablation.

f_{rep} / kHz	P / mW	v / mm/s	R	λ / nm
20	151 / 191 / 268	200	50	1030

The laser beam was focused using a telecentric f-theta lens with a focal length of $f_L = 100$ mm and was controlled using a scan head (Scanlab GmbH). The distance between the focusing lens and the workpiece was varied using the z-axis where the scan head was mounted. Each micro structure was manufactured by ablating lines with 50 repetitions. Figure 1 schematically illustrates the laser system.
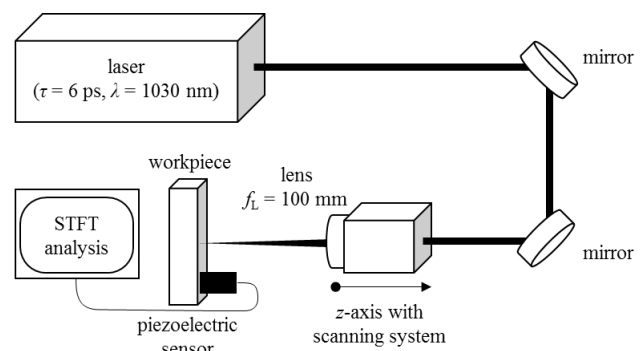

Fig. 1. Schematic view of the laser system.

Three micro structures were ablated for each parameter configuration and were analyzed according to DIN EN ISO 25178 using confocal light microscopy μSurf and the μsoft analysis software of the company Nanofocus AG. In Fig. 2, the topography of ablated microgrooves with varying z-axis position is illustrated exemplarily.
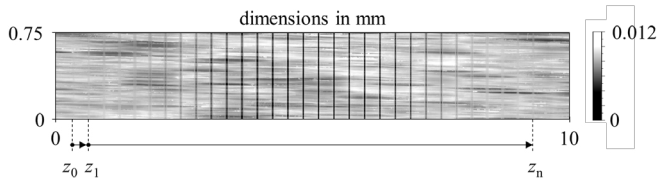
Fig. 2. Topography of ablated microgrooves with varying z-axis position.

Surface topography measurement was performed using a magnification of 20x resulting in a field of view of 750 µm x 750 µm. Using the stitching function each parameter field was measured as a whole and a cross section series of the ablated microgrooves consisting of 456 profiles was implemented. On the basis of the cross-section series the average profiles were calculated and evaluated regarding structure width w and structure depth h.

Measured acoustic emission (AE) signals during laser ablation were analyzed and correlated with surface topography and z-axis position in Section 5.2. AE measurement during laser processing was carried out using the piezoelectric sensor O-WT 232 from QASS GmbH which is a flat frequency response sensor with high sensitivity in the range between 5 Hz and 2 MHz. It was directly mounted on the workpiece. For signal recoding and data storage, the AE analyzing device Optimizer4D (QASS GmbH) was used with a sample rate of $f_s = 3.125$ MHz. The evaluation of the measured raw data was carried out with Matlab software.

3. Effect of laser beam characteristics on ablated structure

The theoretical correlation between the energy density of the laser beam, the beam radius and the radius of the ablated structure depending on the z-axis position is illustrated in Fig. 3.

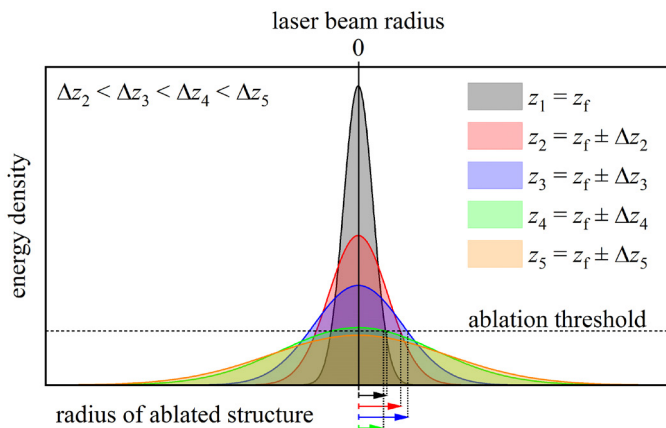Fig. 3. Schematic illustration of the correlation between energy density, laser beam radius and radius of the ablated structure depending on the z-axis position.

An ideal Gaussian laser beam intensity profile and a constant laser power are assumed. In order to ablate workpiece material a laser beam's energy density exceeding the workpiece specific ablation threshold is mandatory. It is known that in the focal position z_f the beam's peak energy density shows the maximum value while the beam's radius shows the minimum value. The radius of the ablated structure

depends on the irradiated area on the workpiece showing energy densities exceeding the ablation threshold. As a consequence, the radius of the ablated structure must have a local minimum for the focal position z_f. There are conditions were the ablated structure radii can be lower compared to those which occur during laser ablation with z_f. These are lower for energy densities slightly exceeding the ablation threshold. Furthermore, a symmetric correlation between the ablated structure radius and a defocusing in both directions can be concluded. Since z_f shows the highest peak of energy density the maximum structure depth is expected.

4. Signal processing

Raw sampled AE data $x[n] = x(n\,t_S)$, $n \in \mathbb{N}$ with sampling time t_S and signal length N are filtered with a bandpass to eliminate irrelevant signal portions of high energy arising from the laser generator, fan or other acoustic sources in the environment that induce vibrations in the workpiece or the sensor. The implementation of laser ablation parameters revealed irrelevant signal components in a frequency range of less than 10 kHz and above 250 kHz, because only within those frequency limits periodically varying signal intensities can be obtained during the laser ablation process. In Fig. 4, an exemplary sequence of raw AE data during the ablation of one line is illustrated.
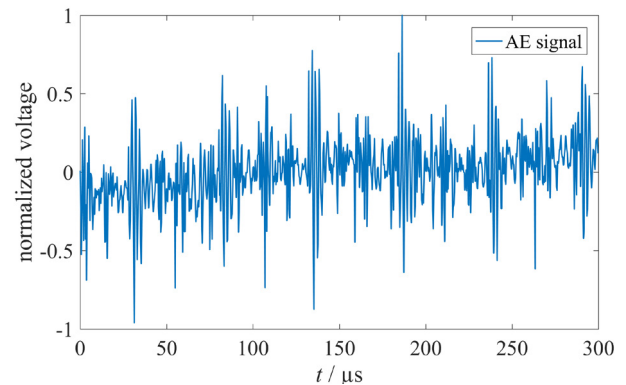

Fig. 4. Typical AE signal measured by the piezoelectric sensor.

The filtered AE data are converted into time-frequency representation with K frequency bins by discrete short-time Fourier transform (STFT). Thus, spectral analysis of the transient signals can be realized time-dependently. Discrete STFT is calculated by

$$E_x^\gamma[m,k] = \sum_{n=0}^{N-1} x[n]\,\gamma_{mk}^*[n] \qquad (1)$$

In this equation, $\gamma_{mk}^*[n]$ is a conjugate complex, time and frequency shifted analysis window:

$$\gamma_{mk}^*[n] = \gamma^*\left((n - m\,\Delta M)t_S\right)e^{-j2\pi kn/K} \qquad (2)$$

The function $\gamma(t)$ is a Gaussian window of range $t \in [-2.5\sigma, 2.5\sigma]$, where $\sigma = 0.262$ ms represents the standard deviation of $\gamma(t)$. In order to transform the entire AE data, $\gamma(n\,t_S)$ is shifted in time for $m \cdot \Delta M$ sampled data points of sampling time t_S, where $\Delta M \cdot t_S$ corresponds to the half of the window size. Consequently, each window is $\Delta t = 1.31$ ms

wide and overlaps half of the neighbor windows. In equation (1), m is the discrete time index of STFT and the index k represents defined frequencies, up to maximum frequency index $K-1$. Both time and frequency data points are scaled equidistantly. Exemplarily, the absolute values of STFT of acoustic emissions during the ablation of a microgroove line are illustrated in Fig. 5.
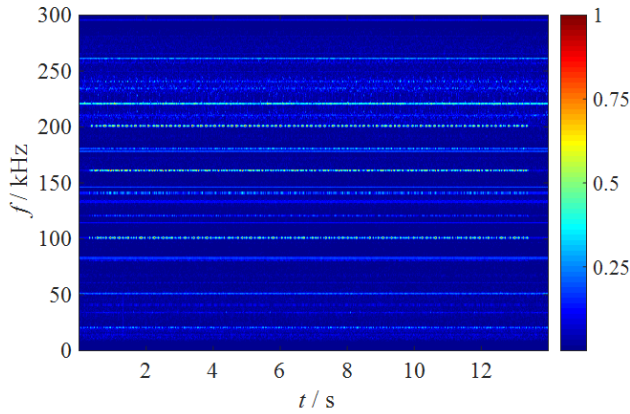

Fig. 5. Time-frequency representation of AE signals during laser ablation process with focal position at z-axis value of -163.1 mm, values normalized.

Ablation is operated between 0.5 and 13.5 s. During this period, intense signal portions can be detected for several frequencies that are multiples of the pulse frequency $f_{rep} = 20$ kHz (i.e. 100 kHz, 120 kHz, 140 kHz, 160 kHz, and 200 kHz in Fig. 5). Furthermore, other intense signal portions can be identified, which do not only occur during laser ablation process, but during the entire signal acquisition time (i.e. 50 kHz, 80 kHz, 180 kHz, and 220 kHz in Fig. 5). Those signal portions represent noise from the environment and are irrelevant in our analysis. All frequencies with intense signal portions remain unchanged for different z-axis positions. In order to exploit the relevant signal portions and to increase signal-to-distortion ratio, STFT values of frequency ranges around the appropriate relevant frequencies are extracted and summed up over the frequency range with indices from k_{min} to k_{max}.

$$s_{FR}[m] = \sum_{k=k_{min}}^{k_{max}} \left| E_x^\gamma[m,k] \right| \qquad (3)$$

The summed signals $s_{FR}[m]$ represent new 1D-signals over time with concentrated information about the ablation process.

For further analysis, fast Fourier transformation (FFT) is performed on those new signals $s_{FR}[m]$ to extract signal components correlating with periodicity of microgroove line ablation. As lines are ablated in several layers, ablation is performed layer by layer with 7.619 Hz periodicity, each layer in 0.13 s. During this ablation process, variances of the AE signal due to different structure depth are neglected, because the ablated structure depth is about ten times smaller than the resolution of the z-axis position. All peaks of FFT absolute values $|S_{FR}[k]|$ corresponding to this periodicity or its multiples are summed to the resulting ablation intensity value I_{FR}.

$$I_{FR} = \sum_{i \in} \left| S_{FR}[i \cdot 7.619\,\text{Hz}] \right| \qquad (4)$$

5. Results

5.1. Analysis of surface topography

Figure 6 shows the measured structure widths w and structure depths h in dependency on the z-axis position which was used for the ablation of microgrooves.
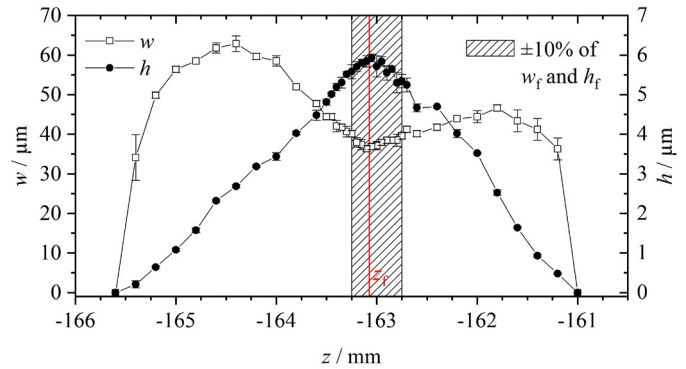

Fig. 6. Evaluated structure depths and widths in dependency on the position of the z-axis.

As expected, structure widths w show a local minimum and structure depths h show a maximum value for a distinct z-axis position indicating the focal position z_f being at a z-axis value of -163.08 mm. Structure dimension w at z_f shows a value of 37 ± 0.75 µm and correlates well with d_f described in section 2. In contrast to the theoretical considerations mentioned, measured results of structure widths w show an asymmetrical distribution. The reason for the asymmetry can be explained by the laser beam profile. In order to draw a conclusion regarding the laser beam profile dimple structures were ablated using the same laser parameters but with a negative pulse overlap as seen Fig. 7.
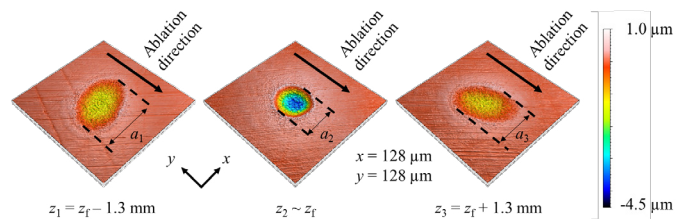

Fig. 7. Surface topography of ablated dimples for defined positions of the z-axis.

The asymmetric distribution of the structure width w in dependency on the z-axis position (Fig. 6) results from the laser beam profile which varies within the tested range of the z-axis positions. Small deviations in the beam path alignment are related to this. Structure width w is determined by the focal spot dimension projected in the ablation direction. According to Fig. 7 it is obvious that the ablated dimension projected in ablation direction a_1 shows a bigger value in comparison to a_3 and thus is consistent to the results in Fig. 6. The circularity as well as the shape of the dimple structure for the focal position z_f indicates a Gaussian intensity profile.

In order to conduct precise laser ablation independently from the ablation direction, a rotationally symmetric beam profile as well as the ensured focal position at any point in time represents basic prerequisites. Especially the adjustment of the focal position during laser ablation on complex shaped workpieces represents a major challenge. Here, the permitted shape deviation depends on the application. For the conducted experiments a permitted shape deviation of $\pm 10\%$ was defined and represents the requirements on the capability of the focal position control system (Fig. 6).

5.2. Analysis of acoustic emission signals

Acoustic emission is generated during laser ablation and therefore it is strongly associated to the laser-material removal process. The dynamics of this removal process are mainly governed by the optical intensity of the laser beam and therefore the energy density exceeding the ablation threshold which are dependent on the focal position [11]. Consequently, AE signals show a high suitability in assessing information about the focal position.

Signal processing of the sensed AE data is executed as presented in Section 4. Relevant frequency ranges with intense absolute STFT values during the ablation process are determined for further analyses and are listed in Table 2.

Table 2. Frequency ranges for AE signal extraction and further processing.

Frequency range No.	1	2	3	4	5	6
f_{min} / kHz	75	98	117	137	155	195
f_{max} / kHz	90	105	123	143	165	205

Three experiments with different laser powers were conducted to investigate the correlation between laser power P and the calculated intensity value I_{FR} of the AE signals. The lens was held in a fixed z-axis position of $z_f = -163.1$ mm. In Fig. 8, the resulting intensity values are displayed for all frequency ranges.
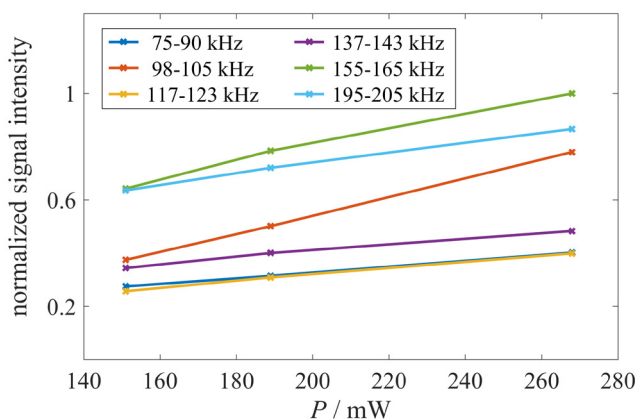

Fig. 8. Calculated intensity values for AE signals of an ablation with $z_f = -163.1$ mm and for all frequency ranges.

As the resulting diagrams for the frequency ranges form straight lines, a proportional correlation between calculated intensity values I_{FR} and laser power can be assumed. This assumption was validated by two additional experiments with varied laser power showing similar results.

In order to analyze the correlation between z-axis position and the occurring AE signals during laser ablation, two micro structures were ablated for each z-axis position between -166.8 mm and -160.4 mm with step size 0.2 mm. The resulting intensity values I_{FR} have been calculated for the defined frequency ranges as described in Section 4. As the portion of relevant signal intensity varies severely in each frequency range, no single frequency range that correlates directly with the z-axis position of the ablation process can be identified. Consequently, the sum of all frequency range-dependent intensity values I_{FR} is considered for each z-axis position. Fig. 9 illustrates the sum of the normalized signal intensity values I_{FR} of the AE signals for the two ablated micro structures by a range between minimum and maximum value compared to the structure depth and width measured by confocal light microscopy in dependency of positions of the z-axis.
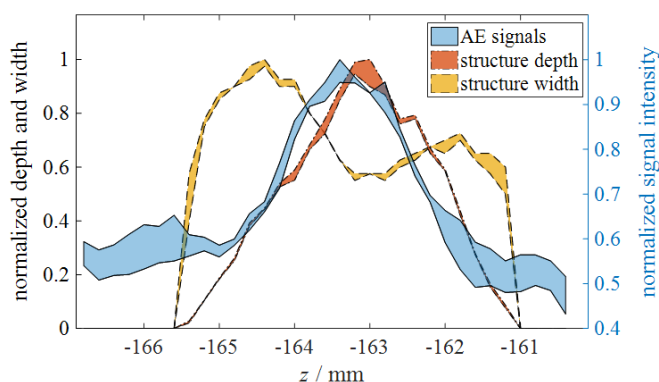

Fig. 9. Normalized signal intensity ranges of the AE signals and normalized structure depth and width ranges in dependency on the position of the z-axis.

A correlation between the focal position and the intensity values calculated from the AE signals can be stated. In the area of focal position with the highest measured structure depth at $z = -163.2$ mm, the intensity values of the AE signals are high as well and exhibit similar variances. For z-axis positions distant from optimal focus, a smaller amount of intensity is measured. Thus, the presented signal processing is suitable to detect the focal position with a maximum deviation of 0.4 mm. The smaller intensity values calculated for z-axis positions distant from z_f occur due to noise or laser excitation without material ablation in the considered frequency ranges. An overall value for the maximum intensity of the AE signals is detected at the z-axis position $z = -163.4$ mm. This value is 0.2 mm (one step lower than the maximum structure depth) and 0.4 mm (two steps lower than the local minimum of structure width). This shift to lower positions can be explained by the influences of structure depth and width on the acoustic emission. Wider and higher structures cause more emissions as a result of more ablation. As the structure width shows an asymmetrical distribution, the emitted energy is asymmetrical as well. Combined with the relatively symmetric structure depth, results of the AE signals are shifted towards the areas with wider ablated structures.

In order to investigate the confirmed correlation of ablated microgrooves and AE signals around the focal position in Fig. 9, additional experiments with a finer resolution of a step size of 50 µm for the z-axis position were conducted. The

resulting normalized AE signal intensities and the optical measured structure depths and widths for the finer z-axis resolution are presented in Fig. 10. Three experiments were conducted for each z. The standard deviation is illustrated by an error bar around the mean value.
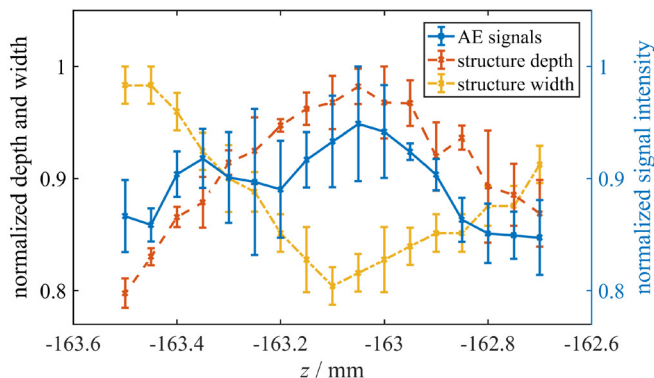

Fig. 10. Normalized signal intensity of the AE signals, structure depth and structure width in dependency on a small area around the focal position with error bars for standard deviation.

The maximum value for the normalized AE signal intensity is calculated for the z-axis position $z = -163.05$ mm, for which the maximum structure depth has been measured, too. Consequently, a strong relation between focal position and AE signals can be noted and focal position can be detected indirectly by the mean value of several AE signal intensities. As the structure width asymmetry in these experiments is not as distinct as in Fig. 9, no shift is detected for the AE signal results. A disadvantage is the high standard deviation for each z-axis position, because robust in-process focal position detection with a deviation smaller than 0.4 mm is impossible without calculation of a mean value for several measurements. With the help of mean values the $\pm$ 10% or 0.2 mm deviation from focal position as a requirement for a focal position control system can be reached.

6. Conclusion

Ablated microgrooves were analyzed by confocal light microscopy to investigate the influence of the z-axis position on the ablated surface geometry. At the focal position the locally deepest and narrowest structure occurs. For varying z-axis position an asymmetrical distribution for the width of the ablated structure can be detected.

In order to control focal position in-process, acoustic emissions were measured and processed further to extract sensitive signal components. First, STFT is calculated for the measured signal and relevant frequency ranges for focal sensitivity are defined. Second, the signal components of the defined ranges are extracted and intensity values are calculated for each range. A proportional correlation between calculated intensity values and laser power can be seen. Furthermore, a strong correlation between focal position and the sum of the calculated intensity values can be detected. The

intensity values exhibit large variances. Thus, mean values have to be calculated to reach a maximum deviation of 0.2 mm enabling in-process focal position detection.

Further improvements are needed in robust signal intensity extraction, because the large uncertainties have to be reduced for reliable focal position detection by acoustic emissions without calculation of mean values. Subsequently, an in-process focal position control can be developed to set focal position to its optimum automatically. Moreover, the dependence of the AE signals on the location of the piezoelectric sensor in relation to the AE source needs to be investigated. Furthermore, the characterization of the influence of the laser power on the uncertainty of the focal position detection is needed. This will be addressed in further studies.

References

[1] Gachot C, Rosenkranz A, Hsu S M, Costa H L. A critical assessment of surface texturing for friction and wear improvement. Wear 2017;372-373:21-41.

[2] Kümmel J, Braun D, Gibmeier J, Schneider J, Greiner C, Schulze V, Wanner A. Study on micro texturing of uncoated cemented carbide cutting tools for wear improvement and built-up edge stabilisation. Journal of Materials Processing Technology 2015;215:62-70.

[3] Fleischer J, Schmidt J, Haupt S. Combination of electric discharge machining and laser ablation in microstructuring of hardened steels. Microsyst Technol 2006;12: 697-701.

[4] Leitz K-H, Redlingshöfer B, Reg Y, Otto A, Schmidt M. Metal Ablation with Short and Ultrashort Laser Pulses. Physics Procedia 2011;12:230-238.

[5] Di Niso F, Gaudiuso C, Sibillano T, Mezzapesa F P, Ancona A, Lugarà P M. Influence of the Repetition Rate and Pulse Duration on the Incubation Effect in Multiple-Shots Ultrafast Laser Ablation of Steel. Physics Procedia 2013;41:698-707.

[6] Cao BX, Hoang PL, Ahn S, Kim J, Kang H, Noh J. In-Situ Real-Time Focus Detection during Laser Processing Using Double-Hole Masks and Advanced Image Sensor Software. Sensors 2017;17:1540.

[7] Cao BX, Hoang PL, Ahn S, Kim J, Noh J. High-precision detection of focal position on a curved surface for laser processing. Precision Engineering 2017;50:204-210.

[8] Fox MDT, French P, Peters C, Hand DP, Jones JDC. Applications of optical sensing for laser cutting and drilling. Applied Optics 2002;41:4988-4995.

[9] Cao BX, Hoang PL, Ahn S, Kim J, Sohn H, Noh J. Real-time detection of focal position of workpiece surface during laser processing using diffractive beam samplers. Optics and Lasers in Engineering 2016;86:92-97.

[10] Schulze V, Weber P, Ruhs C. Increase of process reliability in the micro-machining processes EDM-milling and laser ablation using on-machine sensors. Journal of Materials Processing Technology 2012;212:625-632.

[11] Bordatchev EV, Nikumb SK. Effect of focus position on informational properties of acoustic emission generated by laser–material interactions. Applied Surface Science 2006;253:1122-1129.

[12] Zanger F, Kacaras A, Bächle M, Schwabe M, Puente León F, Schulze V. FEM simulation and acoustic emission based characterization of chip segmentation frequency in machining of Ti-6Al-4V. Procedia CIRP 2018;72:1421-1426.

[13] Liu JM. Simple technique for measurements of pulsed Gaussian-beam spot sizes. Optics Letters 1982;7:196-198.